Red Blood Cell (RBC)-like Ni@N–C composites for Efficient Electrochemical CO_2 Reduction and Zn-CO_2 Battery

Liu Han[a], Cheng-wei Wang[a], Hai-ping Xu[a], Ming Yang[b,c], Bing Li[a], Ming Liu[a]**

[a] School of Chemistry and Chemical Engineering, Harbin Institute of Technology, Heilongjiang Province, 150000, China.

[b.] Department of Applied Physics, The Hong Kong Polytechnic University, Hung Hom, Hong Kong SAR, China.

[c.] Research Centre on Data Sciences & Artificial Intelligence, The Hong Kong Polytechnic University, Hung Hom, Hong Kong SAR, China.

1. Experimental Section

1.1 Materials

Nickel(II) acetate tetrahydrate ($Ni(CH_3COO)_2 \cdot 4H_2O$, ≥99%), 1,10-Phenanthroline monohydrate ($C_{12}H_8N_2 \cdot H_2O$, ≥98%), melamine ($C_3H_6N_6$, ≥99%), cyanuric acid ($C_3H_3N_3O_3$, ≥98%), potassium bicarbonate ($KHCO_3$, ≥99.5%), were all purchased from Aladdin Chemistry Co. Ltd. Dimethyl sulfoxide (C_2H_6SO, ≥99%) and isopropyl alcohol (C_3H_8O, ≥99.5%) were all purchased from Tianjin Fuyu Fine Chemical Co. Ltd.

1.2. Synthesis of Catalysts.

A typical catalyst synthesis process is shown in **Figure 1a**. Melamine (1.00 g) and cyanuric acid (0.80 g) were dissolved in 50 mL of DMSO, respectively. Phenanthroline (0.3171 g) and nickel (II) acetate tetrahydrate (0.0995 g) were added into the cyanuric acid solution and stirred for 10 minutes. Then, the mixed solution was added to the melamine solution continuously stirring for 30 minutes and left undisturbed at room temperature for 2 h. The precipitate was centrifugated, washed with ethanol 3 times, and dried at 60°C overnight. Finally, the precipitate was pyrolyzed at the desired temperature for 2 h with a heating rate of 3°C·min^{-1} in a tube furnace under N_2 flow (100 sccm). The obtained sample was denoted as Ni@NC-T, where T represents the pyrolysis temperature.

1.3. Characterizations

The crystal structure of the as-prepared electrocatalysts were verified by XRD (Bruker-D8, Cu Kα radiation). The morphologies and particle sizes of the catalysts were characterized by scanning electron microscopy (SEM, Hitachi S-4800) and transmission electron microscope (TEM, FEI talos F200S). The chemical state of the electrocatalysts was examined by X-ray photoelectron spectroscopy (XPS, KRATOS AXIS Ultra DLD) and the spectra were calibrated using C1s peak at 284.6 eV. N_2 adsorption–desorption was conducted at 77 K using the ASAP 2020 instrument with degassing samples (200 ℃ for 2 h for the porous structure and surface area characterization. Contact angle measurements were performed on a Biolin Scientific contact angle analyzer.

1.4. Electrochemical measurements

Electrochemical evaluations were performed with an electrochemical workstation (CHI660E). CO_2RR test was carried out in H-type cells with a Nafion-117 proton exchange membrane (gaossunion) to separate the anode and cathode, each chamber contained 30 mL of electrolyte (0.5 M $KHCO_3$ solution) and 20 ml headspace. The KCl solution saturated Ag/AgCl and graphite rod served as reference electrodes and counter electrodes, respectively. Before the electrochemistry test, the $KHCO_3$ solution was purged with 20 mL·min^{-1} CO_2 (> 99.999%) for 30 min. To prepare the working electrode, 5 mg catalysts and 20 μL Nafion solution (5 wt. %) were dispersed into 980 μL of isopropanol solution and sonicated for at least 30 min to generate a well-dispersed catalysts ink. 10 μl ink was loaded onto an L-type glassy carbon electrode with a 5 mm diameter, giving a catalyst loading of 0.25 mg·cm^{-2}. Linear sweep voltammetry (LSV) with 20 mV·s^{-1} was performed in Ar and CO_2-saturated electrolyte stirred at 1000 rpm. The electrochemical impedance spectroscopies (EIS) were recorded at -0.8 V in CO_2-saturated 0.5 M $KHCO_3$ electrolyte under static conditions, with a perturbation amplitude of 5 mV, and a frequency range from 100 KHz to 100 mHz. Cyclic voltammograms (CV) curves were tested in the potential window of 0–0.1 V vs. RHE with different scan rates to obtain double-layer capacitance (Cdl). Chronoamperometry measurements were performed from -0.5 to -1.1 V for 30 min at an interval of 0.1 V.

The gas products were analyzed by an online gas chromatography (GC) system (SCION, 456C) using high-purity Ar (99.999%) as the carrier gas. The liquid products (500 μL electrolyte mixed with 100 μL D_2O and 100 μL dimethyl sulfoxide solution (6 mmol L-1)) were analyzed by Bruker AV400 NMR spectrometer.

The Faradaic efficiency (FE) of the products was calculated as follows:

$$FE = {}^{Q_{product}}\!/_{Q_{total}} = {}^{NZF}\!/_{Q_{toatl}}$$

where N is the moles of product. Z stands for the number of transfer electrons, which was 2 for H_2 and CO, respectively. F is the Faradaic constant (96485 $C \cdot mol^{-1}$); Q_{total} represents the total quantity of electric charge during the whole CO_2 reduction process. The flow-cell measurements were conducted on a three-compartment electrochemical cell. The cathodic and anodic chambers were separated by an anion exchange membrane (Fuma, FAA-3-PK-130). To prepare the working electrode, 100 μL catalyst ink was dispersed on a 2×0.5 cm^2 gas diffusion layer (SGL,29BC) with a 0.5 $mg \cdot cm^{-2}$ catalyst loading. The as-obtained GDE was used as the cathode electrode and a piece of oxidized Ni foam was used as the anode. CO_2 gas flow with the rate of 20 sccm was delivered into the gas chamber. A 1.0 M KOH was circulated to the anode at a flow rate of 5 $mL \cdot min^{-1}$ and cathode electrolytes were circulated by a gas-liquid mixed flow pump. For the stability test, chronopotentiometry at the current density of 100 $mA \cdot cm^{-2}$ was applied.

1.5 Zn-CO_2 battery measurement

The Zn-CO_2 battery was constructed by the flow-cell and the two compartments were separated by a bipolar membrane. The cathodic and anodic electrolytes were 1 M $KHCO_3$ saturated with CO_2 and 6 M KOH solution, respectively. A zinc plate with a geometric area of 6.15 cm^2 was applied as an anode, and the GDL in the flow cell was directly served as a cathode. CO_2 gas flow with the rate of 20 sccm was delivered into the gas chamber and the anode electrolyte was circulated at a flow rate of 1 $mL \cdot min^{-1}$. For the mechanically rechargeable Zn-CO_2 battery, A zinc foil with a geometric area of 1 cm^2 was applied as an anode and fixed with a woodworking clamp.

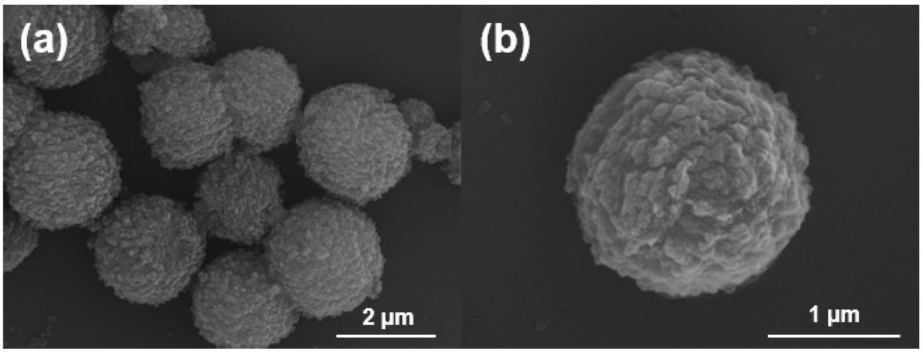

Figure S1. FE-SEM images of chelate-supermolecule complex.

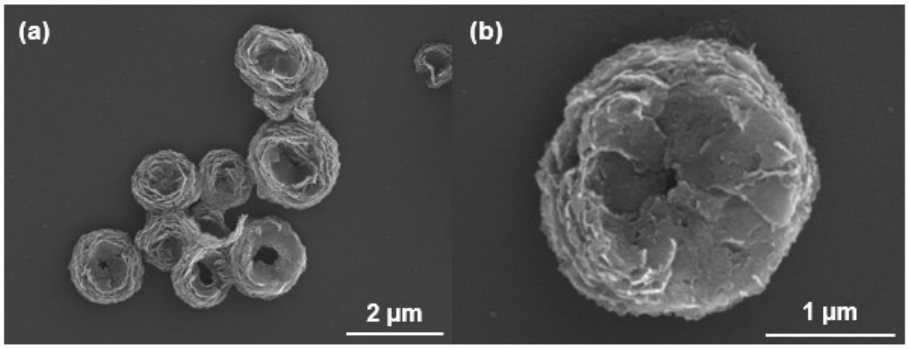

Figure S2. FE-SEM images of Ni@NC-800.

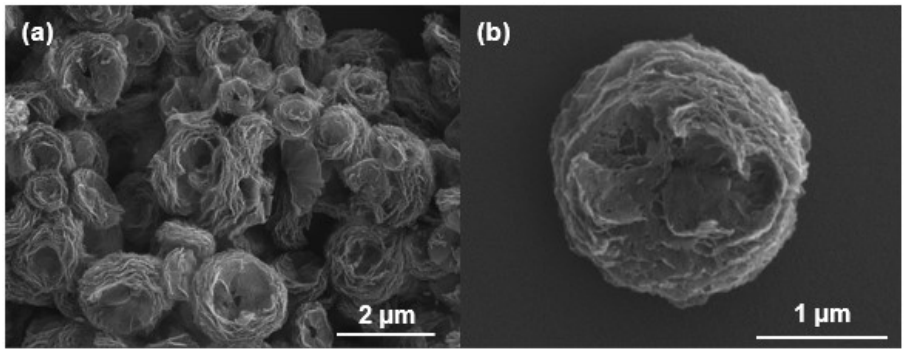

Figure S3. FE-SEM images of Ni@NC-900.

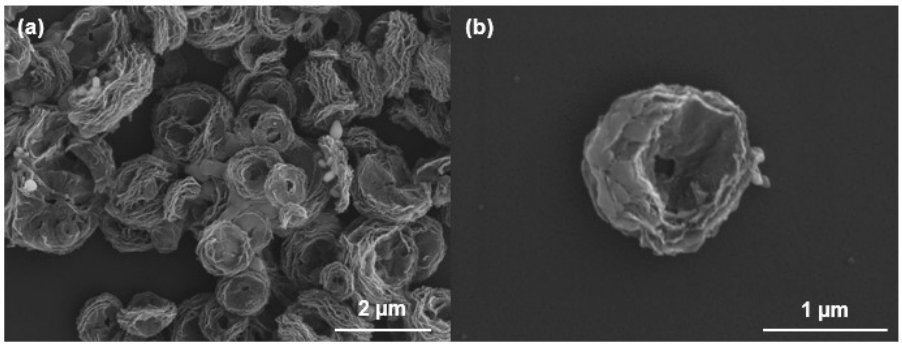

Figure S4. FE-SEM images of Ni@NC-1000.

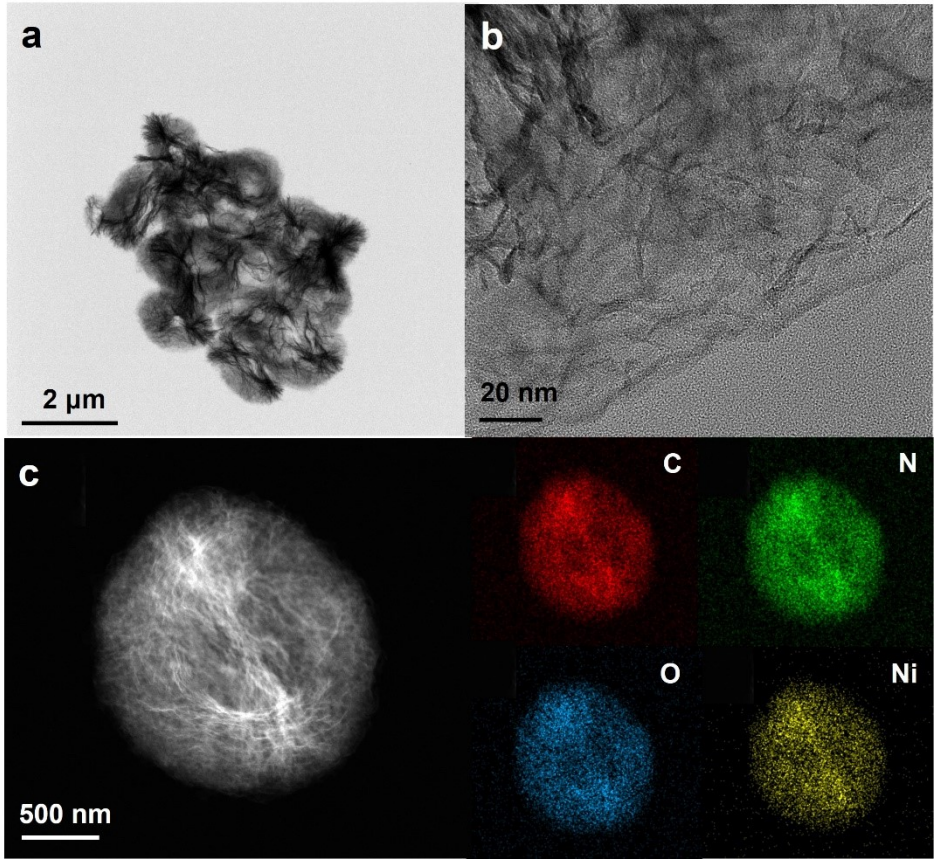

Figure S5. (a) TEM and (b) HRTEM images of Ni@NC-800, and (c) Corresponding EDS mapping of Ni@NC-800 showing the dispersion of C (red), N (green), O (blue), and Ni (yellow).

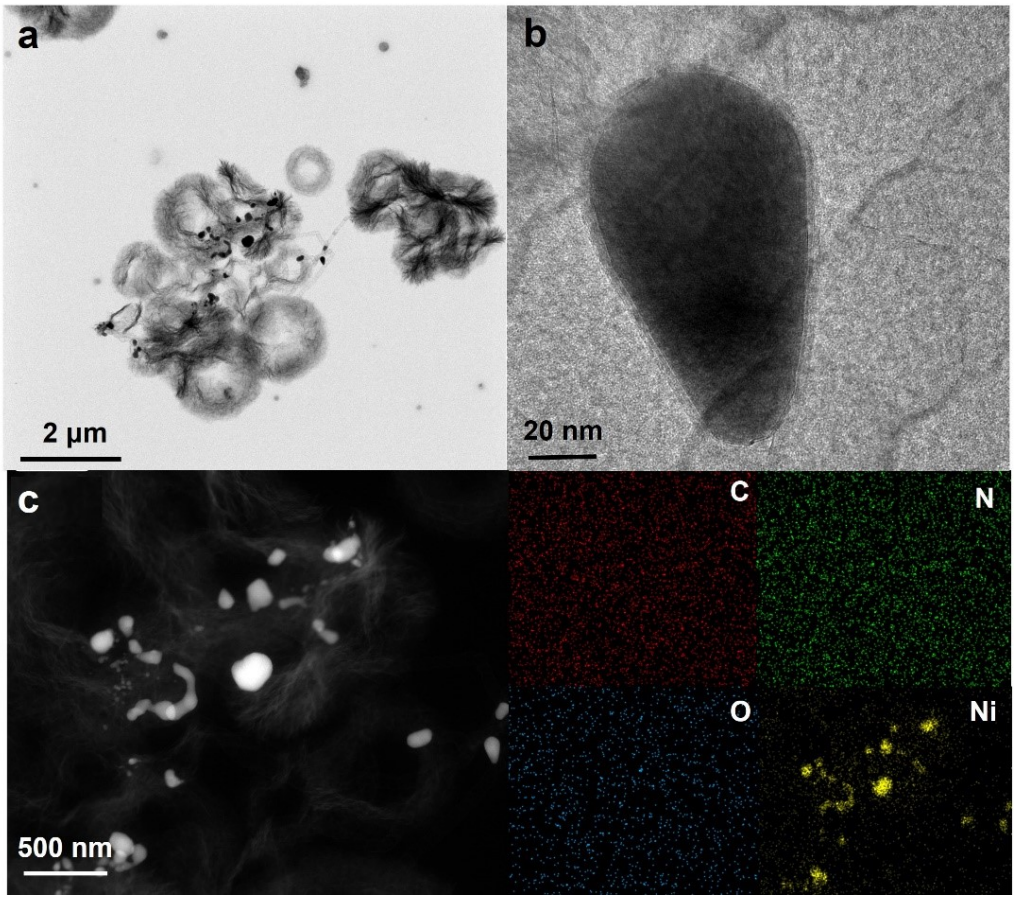

Figure S6. (a) TEM and (b) HRTEM images of Ni@NC-900, and (c) Corresponding EDS mapping of Ni@NC-900 showing the dispersion of C (red), N (green), O (blue), and Ni (yellow).

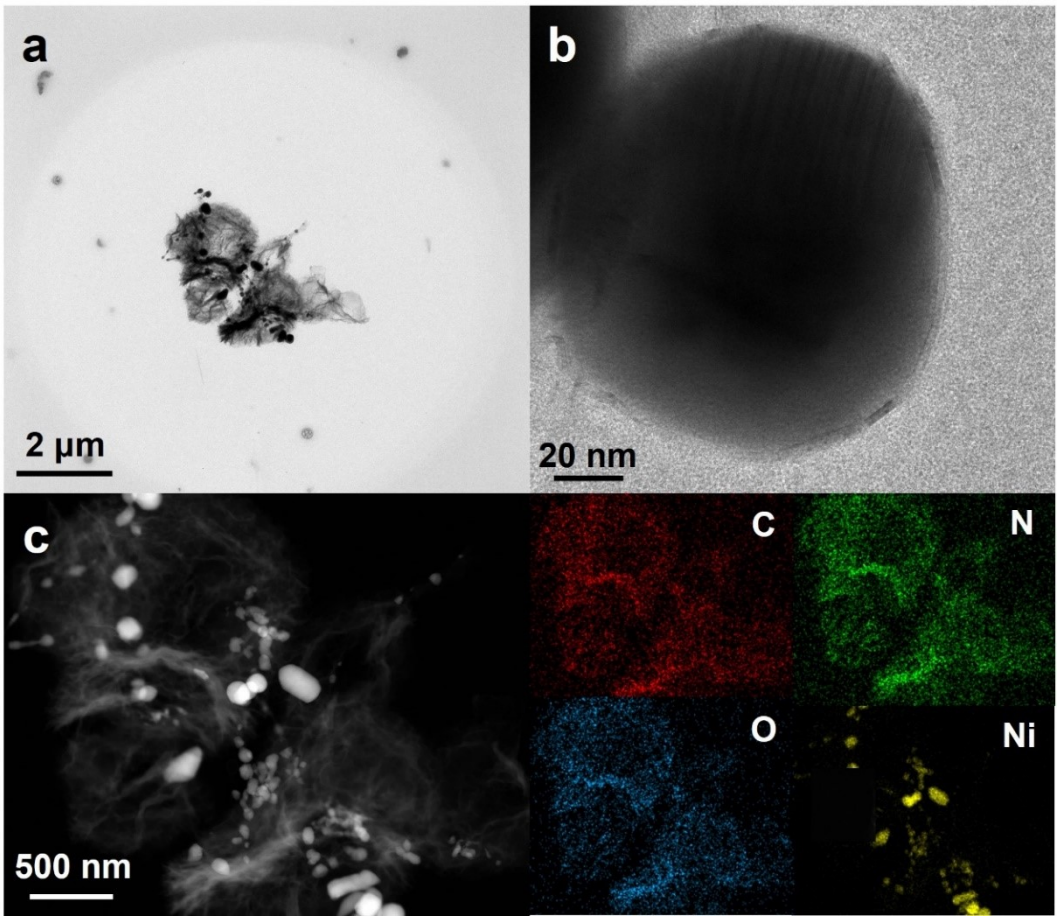

Figure S7. (a) TEM and (b) HRTEM images of Ni@NC-1000, and (c) Corresponding EDS mapping of Ni@NC-1000 showing the dispersion of C (red), N (green), O (blue), and Ni (yellow).

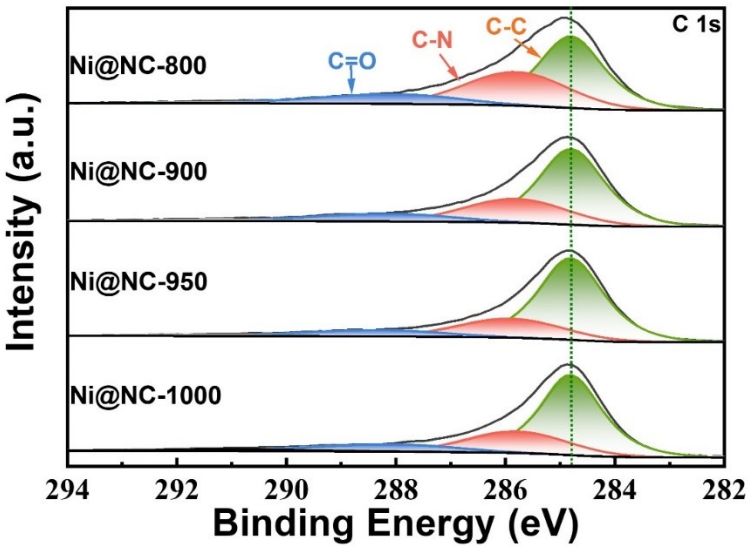

Figure S8. C 1s XPS spectra of four Ni@NC-T samples.

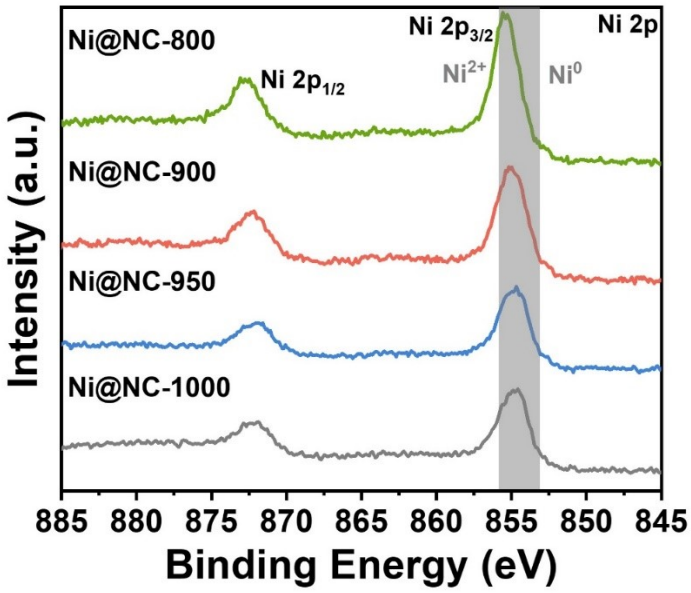

Figure S9. Ni 2p XPS spectra of four Ni@NC-T samples.

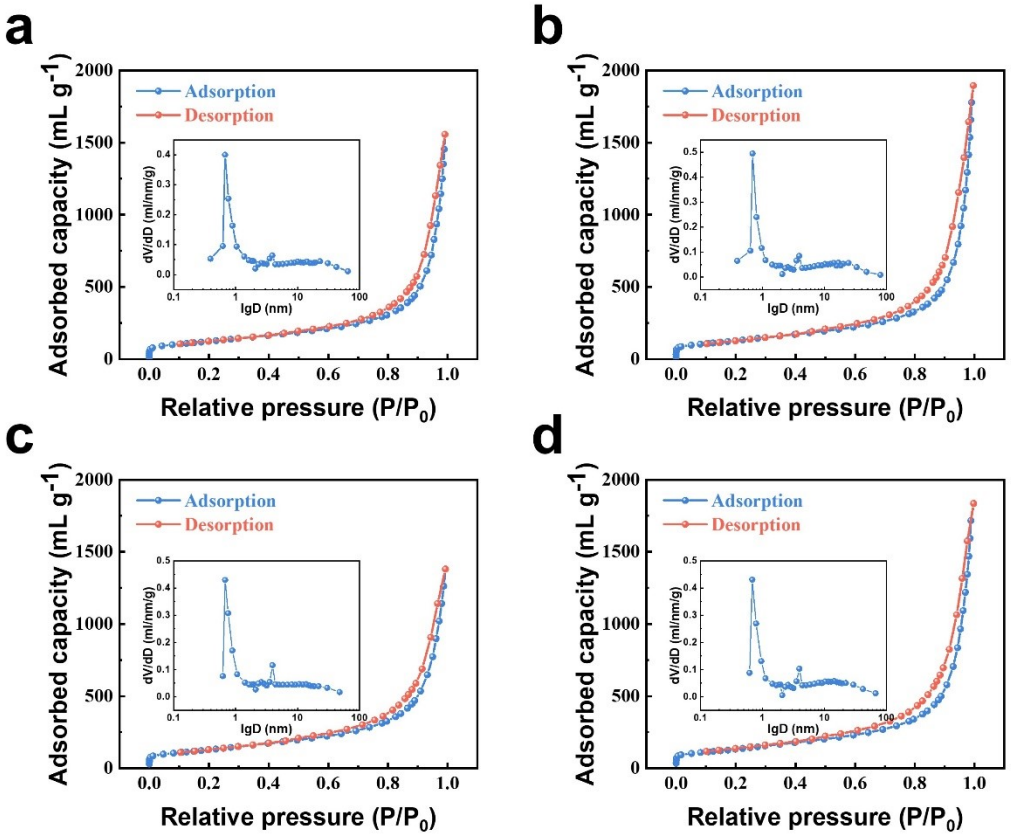

Figure S10. N_2 adsorption-desorption isotherms and the corresponding pore size distribution curve of four Ni@NC-T samples, (a) Ni@NC-800; (b) Ni@NC-900; (c) Ni@NC-950; (d) Ni@NC-1000

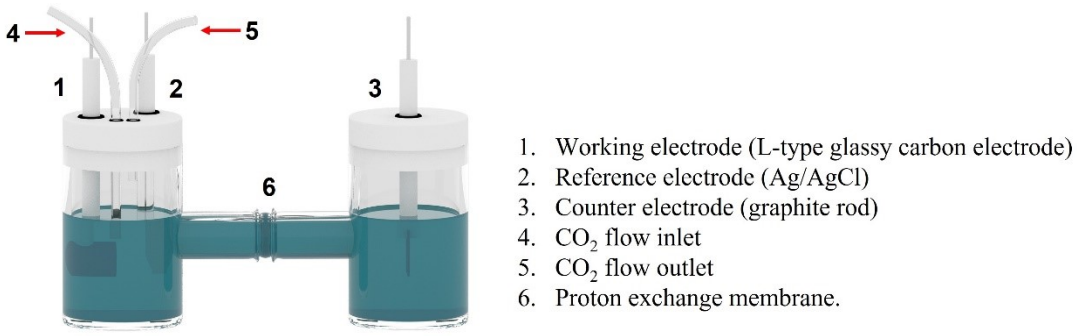

Figure S11. Schematic illustration of traditional H-Cell.

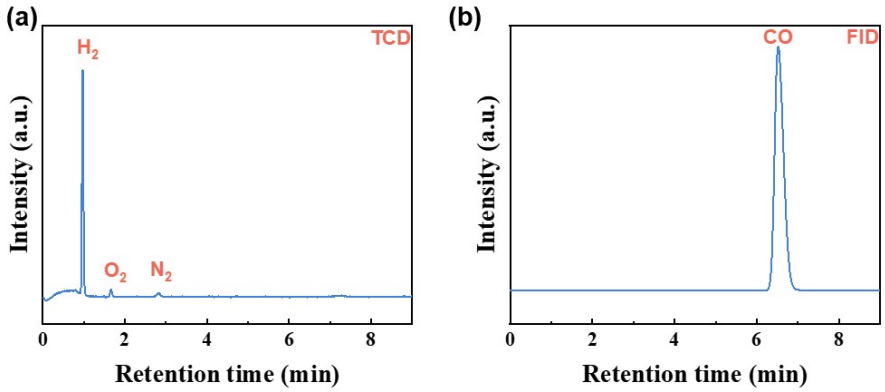

Figure S12. Gas chromatography (GC) analysis of gas products ((a) H_2; (b) CO) released by the Ni@NC-950 sample at -0.8 V.

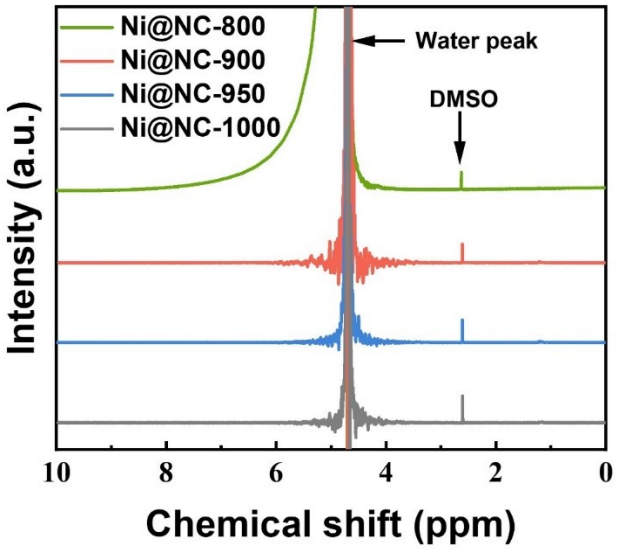

Figure S13. ^{1}H-NMR spectrum of four Ni@NC-T samples for liquid products of accumulated electrolyte at -0.8 V.

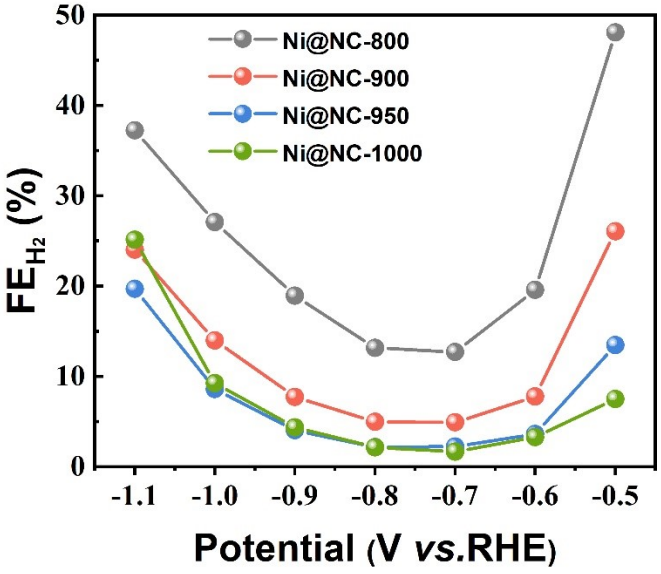

Figure S14. The FE_{H2} of Ni@N-T corresponding to Fig. 2c.

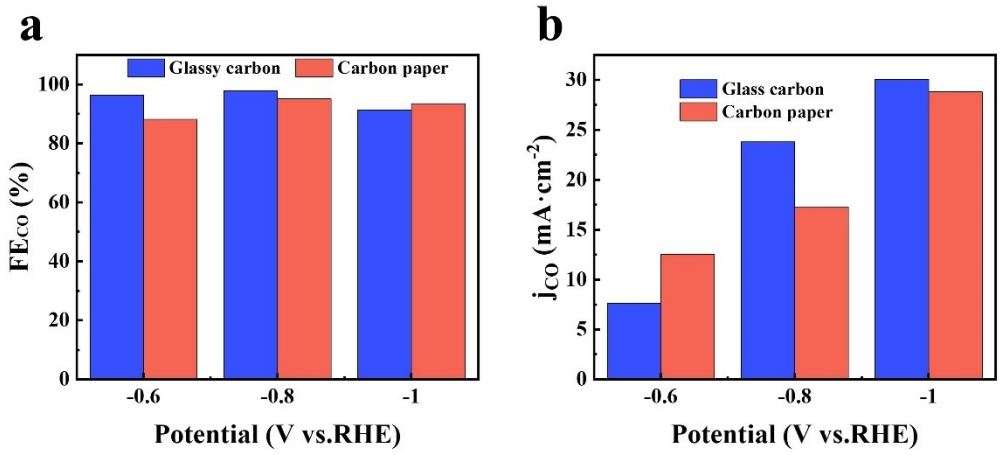

Figure S15. Comparison of a) FE_{CO} and b) J_{CO} when glass carbon electrodes and carbon paper are used as working electrodes in an H-type cell. (The effective working area of carbon paper is 2*1*1 cm^2 with a mass loading of 0. 5 $mg \cdot cm^{-2}$. Other test conditions are consistent with those of the glass carbon electrode.)

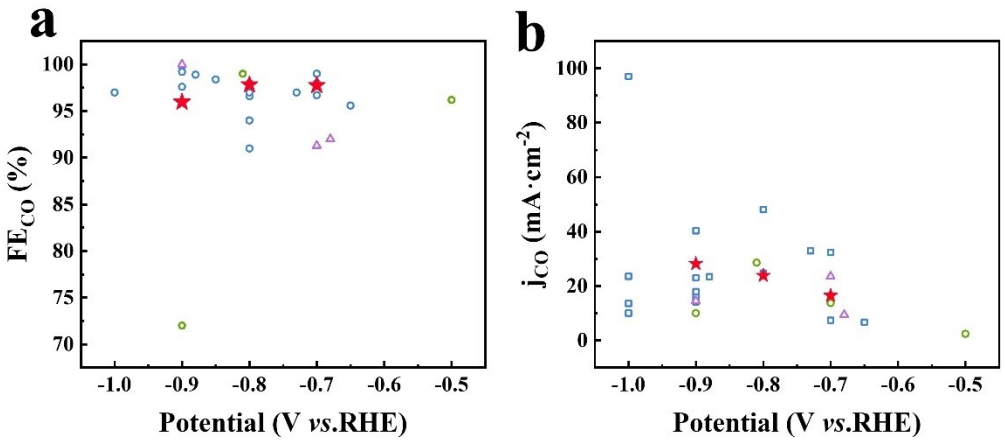

Figure S16. Comparisons of a) FE_{CO} and b) j_{CO} of our synthesized Ni@NC-950 with those of reported typical Ni-based electrocatalysts. To compare the performance of our synthesized catalyst more objectively. We collected the specific journals published over the last 5 years (From 2017 to 2023 years). The blue circle represents the works published in Angewandte Chemie International Edition; The green circle represents the works published in the Journal of the American Chemical Society; The purple triangle represents those published in Advanced Materials and the red star represents our work.

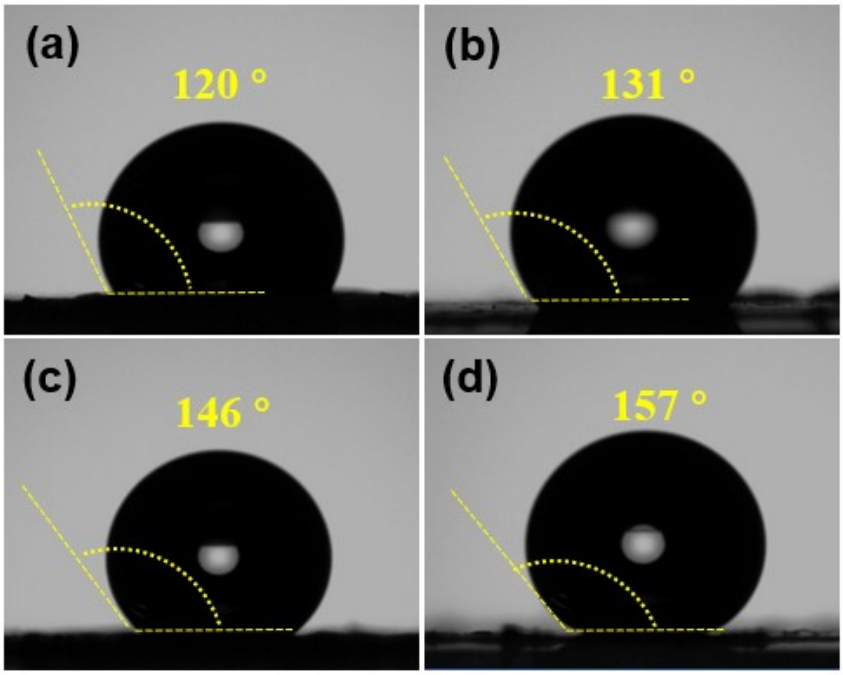

Figure S17. Contact angle tests of (a) Ni@NC-800, (b) Ni@NC-900, (c) Ni@NC-950, and (d) Ni@NC-1000 samples.

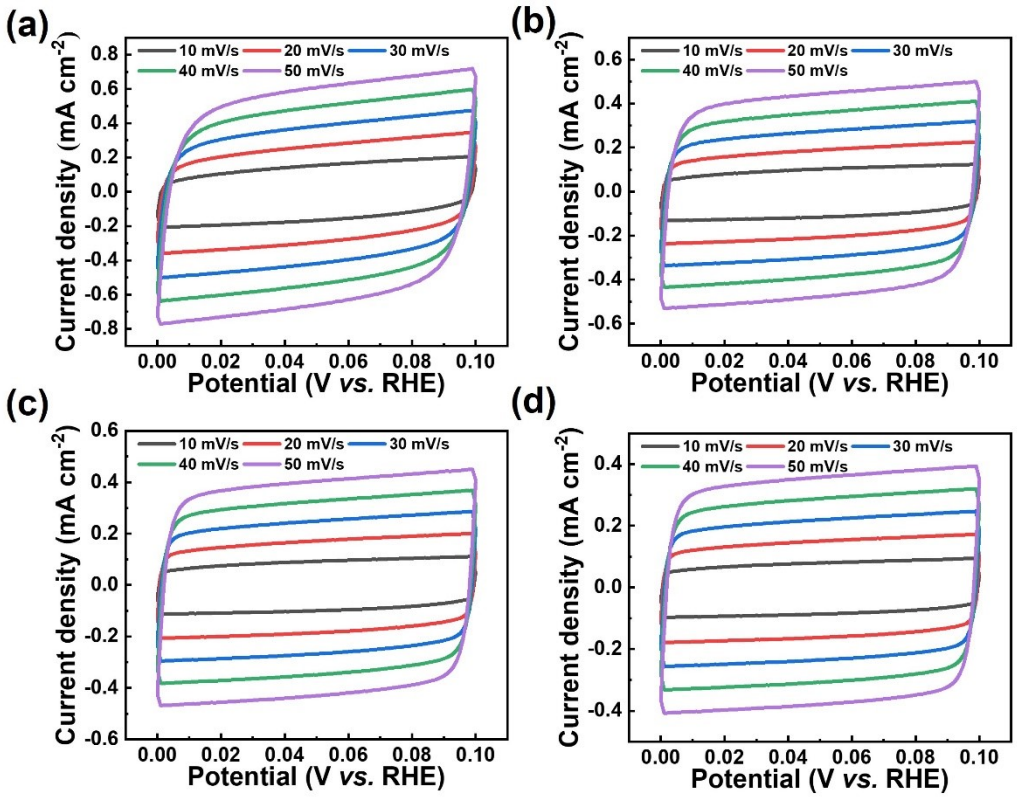

Figure S18. CV curves of (a) Ni@NC-800, (b) Ni@NC-900, (c) Ni@NC-950, and (d) Ni@NC-1000 samples at different scan rates (10, 20, 30, 40, and 50 $mV \cdot s^{-1}$) in a non-Faradaic region from 0 to 0.1 V in the CO_2-saturated 0.5 M $KHCO_3$.

Electrochemical double-layer capacitance (EDLC) measurement was performed on these Ni@NC-T electrodes. Cyclic voltammetry (CV) was performed in the same electrochemical cell during which no Faradaic processes occurred. CV curves were then taken between 0 and 0.1 V vs RHE (Saturated KCl) at various scan rates (mV/s) while keeping the solution still. Then, currents were extracted at 0.05 V vs RHE (Saturated KCl) as a function of the scan rate, leading to a slope for each sample before and after electrolysis. The slope of the plot equals the capacitance of measured the samples.

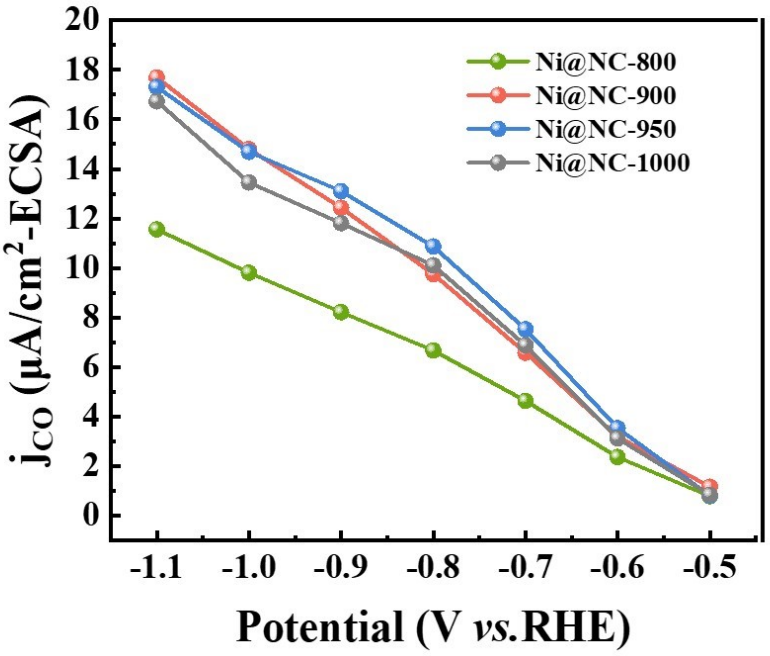

Figure S19. The j_{CO} of Ni@N-T normalized by ECSA.

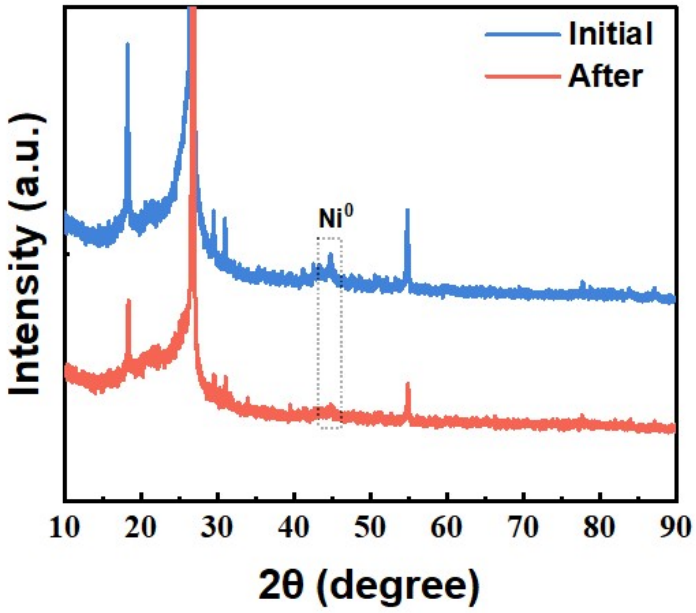

Figure S20. XRD pattern of Ni@NC-950 after CO_2RR. Initial means the fresh catalyst before doing CO_2RR; After means the catalyst was run the CO_2RR for 12 hrs.

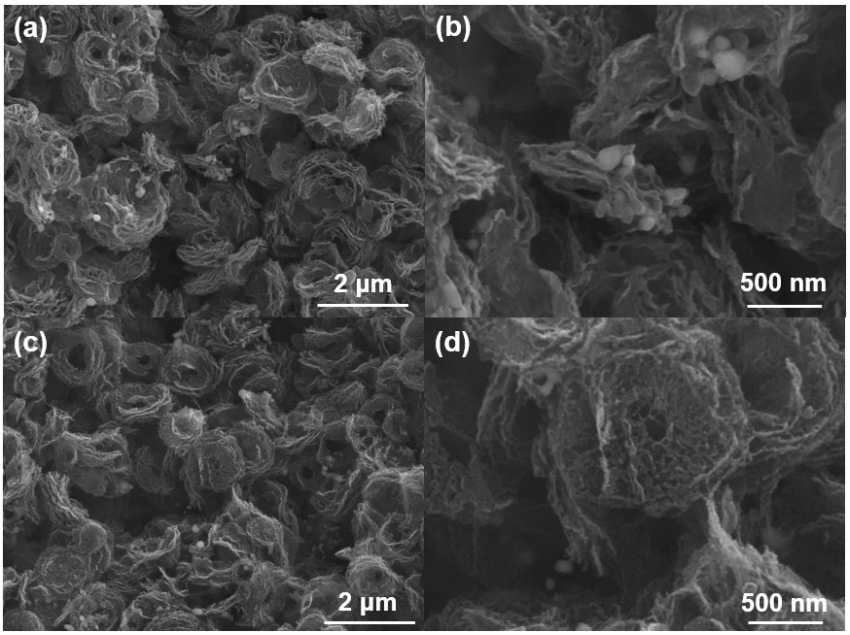

Figure S21. SEM images of Ni@NC-950 before (a, b) and after (c, d) eCO_2RR.

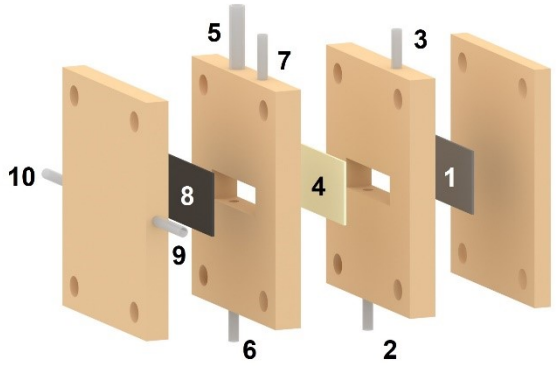

1. Counter electrode (Ni foam)
2. Anode electrolyte inlet
3. Anode electrolyte outlet;
4. Anion exchange membrane
5. Reference electrode (Hg/HgO)
6. Cathode electrolyte inlet
7. Cathode electrolyte outlet
8. Working electrode (catalysts coated)
9. CO_2 flow inlet
10. CO_2 flow outlet

Figure S22. Schematic illustration of the typical flow cell. Step-by-step assembly diagram of the flow cell.

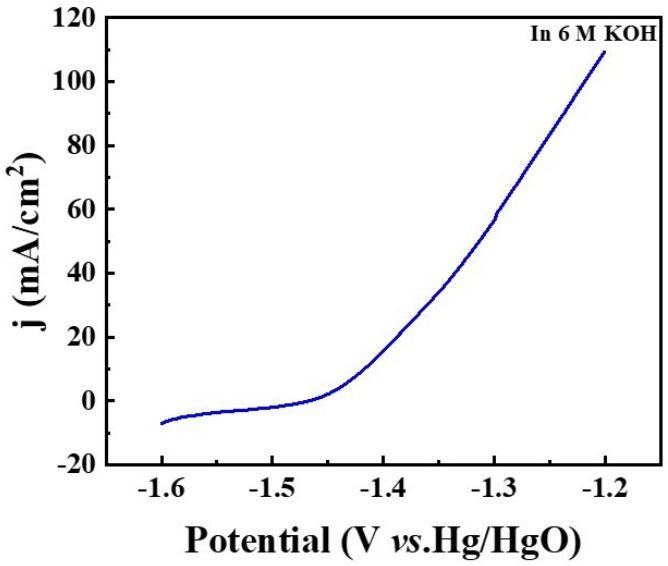

Figure S23. LSV curves of anodic Zn oxidation of Zn plate in 6 M KOH solution (Scan rate: 10 mV/s).

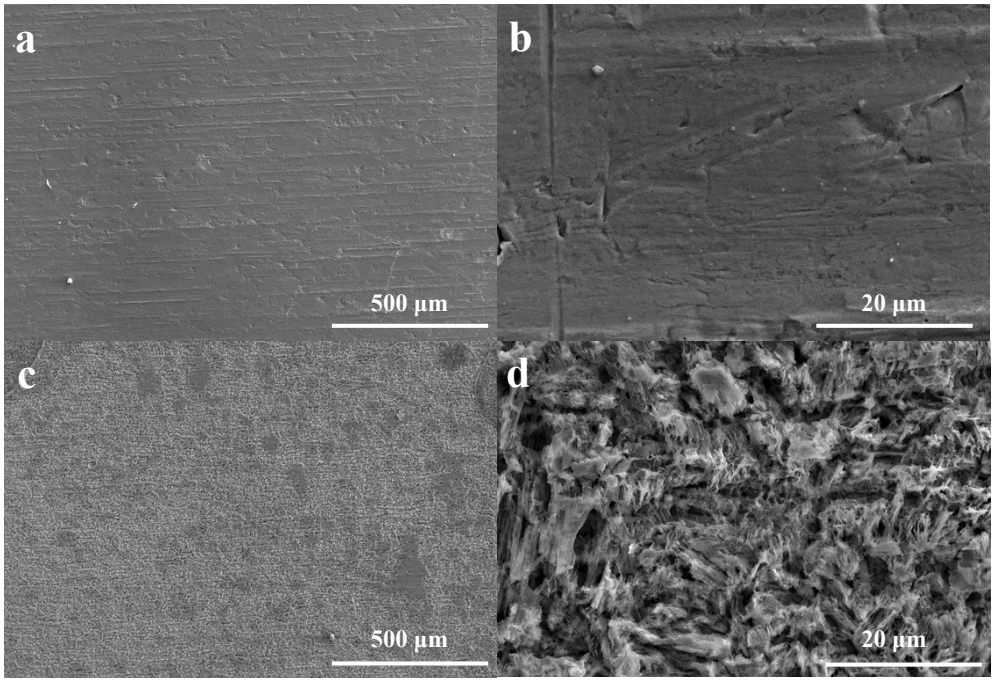

Figure S24.SEM images of Zn plate before (a, b) and after (c, d) discharging 2 hours at 5 mA/cm^2.

Table S1. Summary of the CO Faradic efficiency and CO partial current density for CO_2 reduction on reported catalysts.

Catalysts	Electrolyte	Electrode/Loading (mg/cm^2)	FE_{CO} (E/V vs. RHE)	j_{CO} / $mA \cdot cm^{-2}$ (E/V vs. RHE)	Refs.
Ni@NC-950	**0.5 M $KHCO_3$**	**Glassy carbon (0.25)**	**97.8 (-0.8)**	**23.8 (-0.8)**	**This work**
NiSA-N_2-C	0.5 M $KHCO_3$	Carbon paper (0.6）	98 (-0.8)	/	[1]
Ni-CNT-CC	0.5 M $KHCO_3$	carbon cloth (0.5)	99 (-0.7)	32.3 (-0.7)	[2]
Ni/Fe-N-C	0.5 M $KHCO_3$	Glassy carbon (0.5)	98 (-0.7)	7.4 (-0.7)	[3]
Ni SAs	0.5 M $KHCO_3$	/	98 (-0.8)	10 (-1)	[4]
Ni-N_4-O/C	0.5 M $KHCO_3$	Carbon paper (1)	99.2 (-0.9)	23 (-0.9)	[5]
Ni_2-N_4-C_2	0.5 M $KHCO_3$	Carbon paper (0.5)	96.6 (-0.8)	17.9 (-0.9)	[6]
NiNG-S	0.5 M $KHCO_3$	Carbon paper (1)	97 (-0.8)	40.3 (-0.9)	[7]
Ni-N_3-C	0.5 M $KHCO_3$	Carbon paper (0.6)	95.6 (-0.65)	6.64 (-0.65)	[8]
InNi DS/NC	0.5 M $KHCO_3$	Glass carbon sheets (0.8± 0.1)	96.7 (-0.7)	23.5 (-1)	[9]
Ni-NC(HPU)	0.5 M $KHCO_3$	Carbon paper (0.35)	91 (-0.8)	24.7 (-0.8)	[10]
CBNNiGd-700	0.5 M $KHCO_3$	Carbon paper (1)	97 (-1)	97 (-1)	[11]

$Ni-N_3-V$	0.5 M $KHCO_3$	Self-supported	94 (-0.8)	48 (-0.8)	[12]
NiPc-TFPN COF	0.5 M $KHCO_3$	Carbon paper (1)	99.8 (-0.9)	14.1 (-0.9)	[13]
Ni(I)-NCNT@Ni9Cu	0.5 M $KHCO_3$	Self-supported	97 (-0.73)	32.87 (-0.73)	[14]
Ni-Nx	0.5 M $KHCO_3$	Carbon paper (1)	97.6 (-0.9)	13.5 (-1)	[15]
$NiPc-NiO_4$	0.5 M $KHCO_3$	Carbon paper (0.2)	98.4 (-0.85)	34.5 (-1.2)	[16]
$Ni_2-N_3C_4$	0.5 M $KHCO_3$	carbon cloth (1)	98.9 (-0.88)	23.46 (-0.88)	[17]
Ni_1-N/CNT	0.1 M $KHCO_3$	Carbon paper (0.2)	99 (-0.75)	12 (-0.75)	[18]
Ni_1-N-C	0.5 M $KHCO_3$	Carbon paper (0.3)	96.8 (-0.8)	/	[19]
NiPACN-low	0.1 M $KHCO_3$	Carbon paper (1)	99 (-0.8)	~20 (-0.8)	[20]
$Ni-N_4$	0.5 M $KHCO_3$	Glass carbon sheets (0.2)	99 (-0.81)	28.6 (-0.81)	[21]
Fe_1-Ni_1-N-C	0.5 M $KHCO_3$	Carbon paper (0.3)	96.2 (-0.5)	2.4 (-0.5)	[22]
Ni/Cu−N−C	0.5 M $KHCO_3$	glassy carbon disk electrode (0.255)	97.7 (-0.7)	13.7 (-0.7)	[23]
Ni SAs/N-C	0.5 M $KHCO_3$	Carbon paper (0.2)	72 (-0.9)	10 (-0.9)	[24]
$Ni(-Cl)-N_3O-TPP$	0.5 M $KHCO_3$	glassy carbon disk (/)	80 (-0.65)	/	[25]

NiSA-N-CNTs	0.5 M $KHCO_3$	Carbon paper (1)	91.3 (-0.7)	23 (-0.7)	[26]
Ni^{2+}@N-doped graphene	0.5 M $KHCO_3$	glassy carbon disk (0.3)	92 (-0.68)	9.38 (-0.68)	[27]
Ni-NC(AHP)	0.5 M $KHCO_3$	Carbon paper (0.1)	~100 (-0.9)	14.5 (-0.9)	[28]
NiZn–N_6–C	0.5 M $KHCO_3$	Carbon paper (1)	99 (-0.8)	20.23 (-0.9)	[29]

Table S2. Summary of reported aqueous rechargeable Zn–CO_2 batteries.

Catalysts	**Catholyte**	**Anolyte**	**Power density ($mW \cdot cm^{-2}$) ($j/mA \cdot cm^{-2}$)**	**Product**	**Ref.**
Ni@NC-950	**1 M $KHCO_3$**	**6.0 M KOH**	**2.36 (10.97)**	**CO**	**This work**
NOMC	0.8 M $KHCO_3$	6.0 M KOH with 0.2 M $Zn(CH_3COO)_2$	0.71 (3)	CO	[30]
CoPc@NHCS	0.8 M $KHCO_3$	6.0 M KOH with 0.2 M $Zn(CH_3COO)_2$	1.02 (3)	CO	[31]
Ni–N_4 sites	0.5 M $KHCO_3$	6.0 M KOH with 0.2 M $Zn(CH_3COO)_2$	1.4 (5.3)	CO	[32]
NiFe-DASC	2 M KCl	2.0 M KOH with 0.2 M $Zn(CH_3COO)_2$	1.36 (8.5)	CO	[33]
Fe_1NC/S_1-1000	0.8 M $KHCO_3$	0.8 M KOH with 0.02 M $Zn(CH_3COO)_2$	0.526 (/)	CO	[34]

Cu–N_2/GN	0.5 M $KHCO_3$	6.0 M KOH with 0.2 M $Zn(CH_3COO)_2$	0.62 (1.06)	CO	[35]
I-Ni SA/NHCRs	1 M $KHCO_3$	6.0 M KOH with 0.02 M $Zn(CH_3COO)_2$	2.54 (7.27)	CO	[36]
Fe-N_4O-C/Gr	0.5 M $KHCO_3$	6.0 M KOH with 0.2 M $Zn(CH_3COO)_2$	0.96 (4)	CO	[37]
Bi-D	2 M $KHCO_3$ with 0.02 $HCOO^-$	2.0 M KOH with 0.02 M $Zn(CH_3COO)_2$	1.16 (/)	HCOOH	[38]
Pd1-O-CB	0.5 M $KHCO_3$	6.0 M KOH with 0.02 M $Zn(CH_3COO)_2$	1.72 (7.5)	HCOOH	[39]
SnO_2/MXene	0.1 M $KHCO_3$	1.0 M KOH with 0.02 M $Zn(CH_3COO)_2$	4.28 (13.57)	HCOOH	[40]
PNCB	2 M $KHCO_3$ with 0.02 $HCOO^-$	2.0 M KOH with 0.02 M $Zn(CH_3COO)_2$	1.43 (2)	HCOOH	[41]
BiC/HCS	0.8 M $KHCO_3$	6.0 M KOH with 0.2 M $Zn(CH_3COO)_2$	7.2 ± 0.5 (19.4)	HCOOH	[42]
ZnTe/ZnO@C	0.8 M $KHCO_3$	0.8 M KOH with 0.02 M $Zn(CH_3COO)_2$	0.93 (3)	HCOOH	[43]

Table S3. The Ni-loading in Ni@NC-T was obtained from ICP and EDX

measurements.

Sample	Ni (wt%)-ICP	Ni (wt%)-EDX
Ni@NC-800	0.1082	0.09
Ni@NC-900	0.1038	0.12
Ni@NC-950	0.0987	0.08
Ni@NC-1000	0.0825	0.07

Both EDX and ICP measurements indicate that our samples contain a very limited amount of Ni species, making it challenging to accurately measure its values. Further studies are needed to obtain reliable results in terms of current density relative to the Ni mass loading.

2. References

[1] Y.N. Gong, L. Jiao, Y. Qian, C.Y. Pan, L. Zheng, X. Cai, B. Liu, S.H. Yu, H.L. Jiang, Angewandte Chemie International Edition 132 (2020) 2727-2731.

[2] S. Liu, H.B. Yang, S.F. Hung, J. Ding, W. Cai, L. Liu, J. Gao, X. Li, X. Ren, Z. Kuang, Y. Huang, T. Zhang, B. Liu, Angewandte Chemie International Edition 59 (2019) 798-803.

[3] W. Ren, X. Tan, W. Yang, C. Jia, S. Xu, K. Wang, S.C. Smith, C. Zhao, Angewandte Chemie International Edition 58 (2019) 6972-6976.

[4] Z. Li, D. He, X. Yan, S. Dai, S. Younan, Z. Ke, X. Pan, X. Xiao, H. Wu, J. Gu, Angewandte Chemie International Edition 59 (2020) 18572-18577.

[5] X. Wang, Y. Wang, X. Sang, W. Zheng, S. Zhang, L. Shuai, B. Yang, Z. Li, J. Chen, L. Lei, N.M. Adli, M.K.H. Leung, M. Qiu, G. Wu, Y. Hou, Angewandte Chemie International Edition 60 (2021) 4192-4198.

[6] X. Cao, L. Zhao, B. Wulan, D. Tan, Q. Chen, J. Ma, J. Zhang, Angewandte Chemie International Edition 61 (2021) e202113918

[7] C. Jia, X. Tan, Y. Zhao, W. Ren, Y. Li, Z. Su, S.C. Smith, C. Zhao, Angewandte Chemie International Edition 60 (2021) 23342-23348.

[8] Y. Zhang, L. Jiao, W. Yang, C. Xie, H.L. Jiang, Angewandte Chemie International

Edition 60 (2021) 7607-7611.

[9] Z. Fan, R. Luo, Y. Zhang, B. Zhang, P. Zhai, Y. Zhang, C. Wang, J. Gao, W. Zhou, L. Sun, J. Hou, Angewandte Chemie International Edition 62 (2023) e202216326.

[10] Y. Li, X.F. Lu, S. Xi, D. Luan, X. Wang, X.W. Lou, Angewandte Chemie International Edition 61 (2022) e202201491.

[11] W. Liu, P. Bai, S. Wei, C. Yang, L. Xu, Angewandte Chemie International Edition 61 (2022) e202201166.

[12] X. Rong, H.J. Wang, X.L. Lu, R. Si, T.B. Lu, Angewandte Chemie International Edition 59 (2019) 1961-1965.

[13] M. Lu, M. Zhang, C.G. Liu, J. Liu, L.J. Shang, M. Wang, J.N. Chang, S.L. Li, Y.Q. Lan, Angewandte Chemie International Edition 60 (2021) 4864-4871.

[14] T. Zhang, X. Han, H. Yang, A. Han, E. Hu, Y. Li, X.Q. Yang, L. Wang, J. Liu, B. Liu, Angewandte Chemie International Edition 59 (2020) 12055-12061.

[15] X. Wang, X. Sang, C.L. Dong, S. Yao, L. Shuai, J. Lu, B. Yang, Z. Li, L. Lei, M. Qiu, L. Dai, Y. Hou, Angewandte Chemie International Edition 60 (2021) 11959-11965.

[16] J.D. Yi, D.H. Si, R. Xie, Q. Yin, M.D. Zhang, Q. Wu, G.L. Chai, Y.B. Huang, R. Cao, Angewandte Chemie International Edition 60 (2021) 17108-17114.

[17] Y.N. Gong, C.Y. Cao, W.J. Shi, J.H. Zhang, J.H. Deng, T.B. Lu, D.C. Zhong, Angewandte Chemie International Edition 61 (2022) e202215187.

[18] S. Jin, Y. Ni, Z. Hao, K. Zhang, Y. Lu, Z. Yan, Y. Wei, Y.R. Lu, T.S. Chan, J. Chen, Angewandte Chemie International Edition 59 (2020) 21885-21889.

[19] L. Jiao, W. Yang, G. Wan, R. Zhang, X. Zheng, H. Zhou, S.H. Yu, H.L. Jiang, Angewandte Chemie International Edition 59 (2020) 20589-20595.

[20] D.M. Koshy, S. Chen, D.U. Lee, M.B. Stevens, A.M. Abdellah, S.M. Dull, G.C. Chen, Dennis Nordlund, Alessandro Gallo, Christopher Hahn, Drew C. Higgins, Z. Bao, T.F. Jaramillo, Angewandte Chemie International Edition 59 (2020) 4043-4050.

[21] X. Li, W. Bi, M. Chen, Y. Sun, H. Ju, W. Yan, J. Zhu, X. Wu, W. Chu, C. Wu, Y. Xie, Journal of the American Chemical Society 139 (2017) 14889-14892.

[22] L. Jiao, J. Zhu, Y. Zhang, W. Yang, S. Zhou, A. Li, C. Xie, X. Zheng, W. Zhou,

S.-H. Yu, H.-L. Jiang, Journal of the American Chemical Society 143 (2021) 19417-19424.

[23] J. Zhu, M. Xiao, D. Ren, R. Gao, X. Liu, Z. Zhang, D. Luo, W. Xing, D. Su, A. Yu, Z. Chen, Journal of the American Chemical Society 144 (2022) 9661-9671.

[24] C. Zhao, X. Dai, T. Yao, W. Chen, X. Wang, J. Wang, J. Yang, S. Wei, Y. Wu, Y. Li, Journal of the American Chemical Society 139 (2017) 8078-8081.

[25] H. Kim, D. Shin, W. Yang, D.H. Won, H.-S. Oh, M.W. Chung, D. Jeong, S.H. Kim, K.H. Chae, J.Y. Ryu, J. Lee, S.J. Cho, J. Seo, H. Kim, C.H. Choi, Journal of the American Chemical Society 143 (2021) 925-933.

[26] Y. Cheng, S. Zhao, B. Johannessen, J.P. Veder, M. Saunders, M.R. Rowles, M. Cheng, C. Liu, M.F. Chisholm, R. De Marco, H.M. Cheng, S.Z. Yang, S.P. Jiang, Advanced Materials 30 (2018) 1706287.

[27] W. Bi, X. Li, R. You, M. Chen, R. Yuan, W. Huang, X. Wu, W. Chu, C. Wu, Y. Xie, Advanced Materials 30 (2018) 1706617.

[28] Y. Li, S.L. Zhang, W. Cheng, Y. Chen, D. Luan, S. Gao, X.W. Lou, Advanced Materials 34 (2021) 2105204.

[29] Y. Li, B. Wei, M. Zhu, J. Chen, Q. Jiang, B. Yang, Y. Hou, L. Lei, Z. Li, R. Zhang, Y. Lu, Advanced Materials 33 (2021) 2102212.

[30] S. Gao, Y. Liu, Z. Xie, Y. Qiu, L. Zhuo, Y. Qin, J. Ren, S. Zhang, G. Hu, J. Luo, X. Liu, Small Methods 5 (2021) 2001039.

[31] S. Gong, W. Wang, C. Zhang, M. Zhu, R. Lu, J. Ye, H. Yang, C. Wu, J. Liu, D. Rao, S. Shao, X. Lv, Advanced Functional Materials 32 (2022) 2110649.

[32] W. Zheng, F. Chen, Q. Zeng, Z. Li, B. Yang, L. Lei, Q. Zhang, F. He, X. Wu, Y. Hou, Nano-Micro Letters 12 (2020) 108.

[33] Z. Zeng, L.Y. Gan, H. Bin Yang, X. Su, J. Gao, W. Liu, H. Matsumoto, J. Gong, J. Zhang, W. Cai, Z. Zhang, Y. Yan, B. Liu, P. Chen, Nature Communications 12 (2021) 4088.

[34] T. Wang, X. Sang, W. Zheng, B. Yang, S. Yao, C. Lei, Z. Li, Q. He, J. Lu, L. Lei, L. Dai, Y. Hou, Advanced Materials 32 (2020) 2002430.

[35] W. Zheng, J. Yang, H. Chen, Y. Hou, Q. Wang, M. Gu, F. He, Y. Xia, Z. Xia, Z.

Li, B. Yang, L. Lei, C. Yuan, Q. He, M. Qiu, X. Feng, Advanced Functional Materials 30 (2019) 1907658.

[36] S. Gong, S. Yang, W. Wang, R. Lu, H. Wang, X. Han, G. Wang, J. Xie, D. Rao, C. Wu, J. Liu, S. Shao, X. Lv, Small 19 (2023) 2207808.

[37] S. Chen, J. Chen, Y. Li, S. Tan, X. Liao, T. Zhao, K. Zhang, E. Hu, F. Cheng, H. Wang, Advanced Functional Materials 33 (2023) 2300801.

[38] Y. Wang, Z. Huang, Y. Lei, J. Wu, Y. Bai, X. Zhao, M. Liu, L. Zhan, S. Tang, X. Zhang, F. Luo, X. Xiong, Chemical Communications 58 (2022) 3621-3624.

[39] J. Li, L.-W. Chen, Y.-C. Hao, M. Yuan, J. Lv, A. Dong, S. Li, H. Gu, A.-X. Yin, W. Chen, P. Li, B. Wang, Chemical Engineering Journal 461 (2023) 141865.

[40] L. Han, X. Peng, H.-T. Wang, P. Ou, Y. Mi, C.-W. Paoh, J. Zhou, J. Wang, X. Liu, W.-F. Pong, J. Song, Z. Lin, J. Luo, H.L. Xin, Proceedings of the National Academy of Sciences (2022) e2207326119.

[41] Y. Wang, L. Xu, L. Zhan, P. Yang, S. Tang, M. Liu, X. Zhao, Y. Xiong, Z. Chen, Y. Lei, Nano Energy 92 (2022) 106780.

[42] M. Yang, S. Liu, J. Sun, M. Jin, R. Fu, S. Zhang, H. Li, Z. Sun, J. Luo, X. Liu, Applied Catalysis B: Environmental 307 (2022) 121145.

[43] X. Teng, J. Lu, Y. Niu, S. Gong, M. Xu, T.J. Meyer, Z. Chen, Chemistry of Materials 34 (2022) 6036-6047.